Coupling framework (1.0) for the Úa (2023b) ice sheet model and the FESOM-1.4 z-coordinate ocean model in an Antarctic domain

Ole Richter[1,2,3], Ralph Timmermann[1], G. Hilmar Gudmundsson[2], and Jan De Rydt[2]

[1]Physical Oceanography of Polar Seas, Alfred Wegener Institute, Bremerhaven, Germany
[2]Department of Geography and Environmental Sciences, Northumbria University, Newcastle upon Tyne, UK
[3]Chair of Modelling and Simulation, University of Rostock, Rostock, Germany

Correspondence: Ole Richter (olewelt@gmail.com)

Abstract. The rate at which the Antarctic Ice Sheet loses mass is to a large degree controlled by ice-ocean interactions underneath small ice shelves, with the most sensitive regions concentrated in even smaller areas near grounding lines and local pinning points. Sufficient horizontal resolution is key to resolving critical ice-ocean processes in these regions, but difficult to afford in large-scale models used to predict the coupled response of the entire Antarctic Ice Sheet and the global ocean to climate change. In this study we describe the implementation of a framework that couples the ice sheet flow model Úa with the Finite Element Sea Ice Ocean Model (FESOM-1.4) in a configuration using depth-dependent vertical coordinates. The novelty of this approach is the use of horizontally unstructured grids in both model components, allowing us to resolve critical processes directly, while keeping computational demands within the range of feasibility. We use the Marine Ice Sheet–Ocean Model Intercomparison Project framework to verify that ice retreat and readvance is reliably simulated, and inaccuracies in mass, heat and salt conservation are small compared to the forcing signal. Further, we demonstrate the capabilities of our approach for a global ocean/Antarctic Ice Sheet domain. In a 39-year hindcast simulation (1979-2018) we resolve retreat behaviour of Pine Island Glacier, a known challenge for coarser resolution models. We conclude that Úa-FESOM is well suited to improve predictions of the Antarctic Ice Sheet evolution over centennial time scales.

1 Introduction

Our limited ability to predict the dynamics of the Antarctic Ice Sheet is a main source of uncertainty in projections of future sea level rise (IPCC, 2013, 2021). A large part of this uncertainty stems from the absence of ice sheet-ocean feedback in model predictions, which is critical to robustly determine future loss of grounded ice and the potential onset of ice sheet collapse (e.g. Colleoni et al., 2018; IPCC, 2013).

In Antarctica, coastal processes exert such control over ice sheet evolution, because glaciers terminate into floating ice shelves that buttress grounded ice discharge (e.g. Goldberg et al., 2009; Gudmundsson, 2013; Reese et al., 2018). Ocean-driven melting can thin the ice shelves, leading to reduced buttressing and retreat of the tributary glaciers. Changes in the ice

shelf geometry, in turn, affect ocean circulation and ice shelf basal melting. The response of this coupled system to a warming ocean is complex (e.g. De Rydt and Naughten, 2024) - even in idealised scenarios with simple geometries (Asay-Davis et al.,
25 2016; De Rydt and Gudmundsson, 2016).

Several approaches have been developed to account for the coupled ice–ocean response in ice sheet flow models. Options range from simple parameterisations based on far-field ocean temperature and ice shelf draft to cavity circulation emulators to coupled ocean-ice sheet models (see Kreuzer et al., 2021, for a summary). Coupled models are the most accurate and most expensive option as they resolve the full three-dimensional circulation inside the sub-ice shelf cavity and calculate ice shelf
30 melting based on the ocean conditions right at the ice shelf base. They have been used to study Antarctic Ice Sheet / ice shelf evolution over centennial timescales (Timmermann and Goeller, 2017; Naughten et al., 2021; Siahaan et al., 2022) and to evaluate and tune approaches with simplified coastal dynamics (Favier et al., 2019). Regional applications of coupled models have successfully been used to study the evolution of individual drainage basins. For the entire Antarctic Ice Sheet, however, it is challenging to afford sufficiently high resolution to adequately resolve areas directly downstream of grounding lines, where
35 most of the buttressing is concentrated (Asay-Davis et al., 2016; Siahaan et al., 2022; Hoffman et al., 2023).

Flexibility in horizontal discretisation could help to focus efforts on the critical components. The current mass balance of the entire ice sheet, for example, is heavily affected by the retreat of comparatively few glaciers and largely determined by ice–ocean interaction underneath their small ice shelves (Pritchard et al., 2012; Smith et al., 2020). Melting in these regions is governed by intrusions of warm deep water, which find their path across the continental shelf along a few, specific routes
40 (Nakayama et al., 2019). Finally, some ice shelf parts are more relevant for buttressing than others. The geometry of the ice within a narrow band around the grounding line, for example, is critical for the stress field of the entire ice shelf (Reese et al., 2018) and determines the potential for unstable glacier retreat (Gudmundsson et al., 2012).

To resolve ice flow dynamics at the resolution that is locally required, some ice sheet models use unstructured grids (e.g. see Cornford et al., 2020). This approach has also been successfully applied in several standalone simulations of the ocean (e.g.
45 Timmermann et al., 2012), and for either the ice or the ocean component in coupled ice sheet–ocean models (e.g. Timmermann and Goeller, 2017; Naughten et al., 2021). To the best of our knowledge, however, no coupled model is available yet that exploits the benefits of unstructured meshes in both components at the same time. These benefits can extend beyond resolving critical processes within the individual components. If, for example, the models are configured to solve the governing equations for the ice and ocean on the same mesh, both models see exactly the same geometry and there is no need to interpolate values
50 between the components.

Here, we present a new framework that couples the ice sheet model Úa with the ocean model FESOM. Both components are established tools for large-scale simulations on realistic domains using horizontally unstructured grids. In this study, we describe the technical implementation, verify the code and show how the enhanced mesh flexibility helps to overcome some of the challenges of coupled modelling at large scales. Ultimately, we aim to provide a new tool that can be used to study ice
55 sheet-ocean interaction over centennial time scales.

In the following section, we introduce Úa and FESOM, describe our coupling approach and details of the data exchange, and present selected aspects of the model configuration for this study. In section 3, we verify the code using the well con-

strained idealised configuration of the Marine Ice Sheet Ocean Model Intercomparison Project (MISOMIP1). In section 4, we demonstrate the capabilities of Úa-FESOM in the pan-Antarctic domain under present-day conditions. Section 5 concludes the study.

2 Model description

2.1 Úa

Úa is an open-source ice flow model (Gudmundsson, 2024) that has been used successfully to study ice shelf–ice stream systems in idealised experiments (Gudmundsson et al., 2012; Gudmundsson, 2013), realistic, more complex setups (De Rydt et al., 2015; Gudmundsson et al., 2019) and coupled ocean-ice sheet configurations (De Rydt and Gudmundsson, 2016; Naughten et al., 2021; De Rydt and Naughten, 2024). Further, Úa has participated in model intercomparison projects, such as the third Marine Ice Sheet Model Intercomparison Project MISMIP (Cornford et al., 2020) and the Marine Ice Sheet Ocean Intercomparison Project MISOMIP (Asay-Davis et al., 2016).

The model solves the vertically integrated formulation of the momentum equations on unstructured grids using the finite-element method. Automated mesh refinement and coarsening is used to, e.g., track grounding line positions with high precision as glaciers evolve. Úa is initialised using an inverse approach and, thus, is built to predict ice dynamics efficiently over time scales of decades up to centuries. Fully implicit forward integration with respect to both ice thickness and ice velocities is done using the Newton-Raphson method, while the Active-Set method automatically ensures positive ice thickness in a volume conserving fashion. The impact of horizontal density variations on the force balance is included in the momentum and mass conservation equations (Schelpe and Gudmundsson, 2023). The model uses inversion to directly estimate the value of the rate factor and the basal slipperiness distribution from surface measurements, thereby ensuring that the initial state is in a close agreement with observations.

2.2 FESOM

The Finite Element Sea ice-Ocean Model (FESOM) is a primitive-equation, hydrostatic ocean model developed at the Alfred-Wegener-Institut, Helmholtz-Zentrum für Polar- und Meeresforschung (Wang et al., 2014). FESOM comprises a two-layer dynamic-thermodynamic sea-ice component (Danilov et al., 2015) and thermodynamic interaction at ice-shelf bases using the three-equation melt parameterisation (Timmermann et al., 2012). The model has been used successfully to study ocean-ice shelf interaction in stand-alone setups (e.g. Naughten et al., 2018) and coupled to an active ice sheet (Timmermann and Goeller, 2017). For this study, we use FESOM-1.4 in a global domain with depth-dependent vertical coordinates. In contrast to Úa, FESOM does not allow for at-runtime variations in the computational domain or its discretisation.
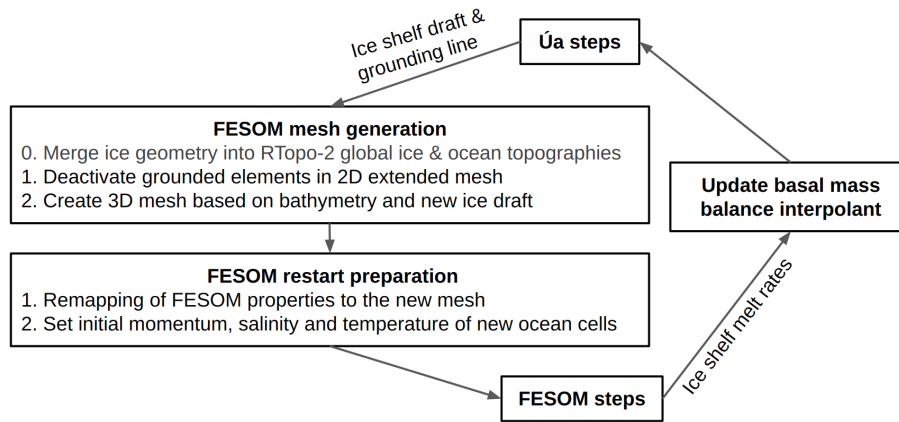
Figure 1. Úa-FESOM coupling scheme. The coupler communicates ice shelf melt rates and ice shelf cavity geometry and initialises new cavity regions. Step 0 of FESOM mesh generation is not used in the idealised experiment.

2.3 Coupling approach

The coupler builds on the infrastructure developed for the Regional Antarctic and Global Ocean (RAnGO) model (Timmermann and Goeller, 2017) and follows a "sequential" approach in that it runs the ice and ocean components subsequently and at different time steps, but eventually covering identical time-spans. The coupling interval is variable at multiples of monthly steps and typically not identical to the forward time-step of either the ocean or the ice-flow model.

Figure 1 outlines one coupling cycle of Úa-FESOM. At each interval, FESOM provides Úa with ice shelf basal melt rates as boundary conditions to compute the ice flow and the evolution of ice thickness. Melt rates are averaged over the time span since the last coupling step and extrapolated in regions that unground during Úa's forward integration using the nearest-neighbour approach in Cartesian space. After integration, Úa returns its final ice shelf thickness and grounding line location to the coupler and a new cavity geometry for FESOM is derived. Prognostic ocean variables are remapped from the end of the last coupling step and extrapolated where the ice has retreated. Subsequently, FESOM is run forward for another coupling interval, and the cycle repeats.

Previous coupling approaches using Z-coordinate ocean models reported numerical instabilities caused by spurious barotropic waves (e.g. Smith et al., 2021; Naughten et al., 2021). These waves arise at the coupling steps due to abrupt changes in ice draft geometry. To mitigate this issue, we implemented a high vertical resolution within the ice shelf cavities and, in the realistic experiment, included an initial adjustment period of 20 years. As a result, ice retreat or readvance during the simulation period rarely exceeds one vertical layer (10-30 m) per coupling step, effectively preventing instabilities associated with spurious barotropic waves.
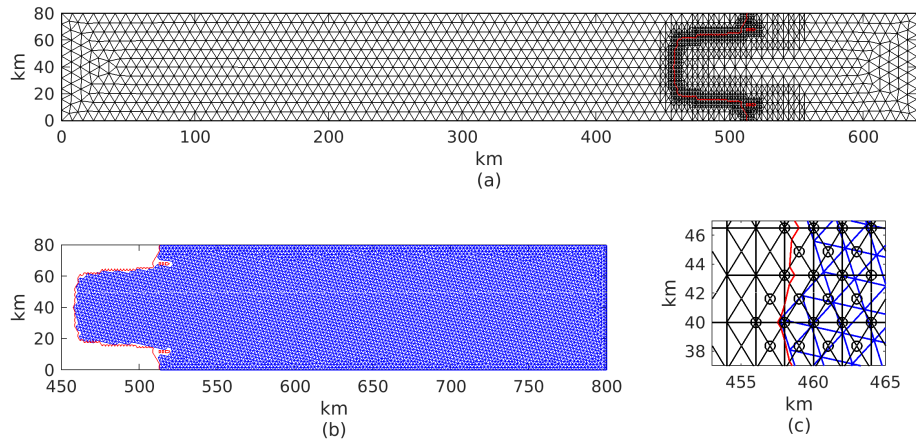
Figure 2. Horizontal grids for the idealised experiment. The marine terminating ice sheet (a) is discretized using 8 km resolution in the background and adaptive mesh refinement around the grounding line with up to 2 km resolution. For the ocean grid (b) we apply a uniform 2 km horizontal resolution. A zoom-in on the grounding zone (c) shows that ice and ocean nodes are not aligned and that ice nodes at which melting is applied (marked by black circles) can extend upstream of the grounding line location used for FESOMs mesh generation (red line).

At each coupling step the models are restarted from their final state at the end of the previous timestep, through the use of restart files. This procedure allows users to run each component of the model system on its most suitable infrastructure. For example, in its configuration presented here, FESOM runs in massively parallel mode on an NHR (Nationales Hochleistungsrechnen) computer, Úa on the AWI supercomputer Albedo and the coupler on an AWI desktop machine. Copying of the relevant data between the machines uses only a small fraction of the overall walltime (see Sec. 4.4) and data transfer and restarts are fully automated using shell scripts. In the following, each part of the coupling routines is described in detail.

2.4 FESOM-to-Úa step

After FESOM has calculated ocean circulation and melt rates for the respective coupling step (i.e as an average over the time span since the last coupling step), the basal mass balance used by Úa for the same time period is updated. Figure 2 shows an example of the horizontal ice and ocean meshes for the idealised MISOMIP1 experiment (Asay-Davis et al., 2016). The geographical node locations in shared regions are not aligned (Fig. 2c) and melt rates are interpolated and extrapolated in Cartesian space using the bilinear and nearest-neighbour approach, respectively. After the interpolation, melt rates are set to zero in fully grounded regions by multiplying them with Úa's grounded/floating mask. The mask is continuously differentiable and, thus, features some regions with values between zero (fully grounded) and 1 (fully ungrounded). Interpolation and masking are repeated at each ice model time step, as Úa's grounding line and mesh evolve during forward integration.

2.5 Úa-to-FESOM step

After Úa has evolved the ice sheet for one coupling time span, the coupler derives a new cavity geometry for FESOM. As a first step, newly grounded (ungrounded) regions are excluded (included) in the horizontal directions of the ocean model domain. This is realised by deactivation (activation) of elements in a two dimensional background mesh, which is generated before the simulation and extends into all regions that could possibly unground during the simulation period. The generation of this mesh is application-specific and further described in Sections 3.2 and 4.2 for the idealised and realistic configuration, respectively. Úa's final grounded/floating mask is interpolated to this background mesh using the linear approach in Cartesian space. We use the median value of this mask (0.5) to define the exact grounding line position for FESOM (red line in Fig. 2). All ocean elements that contain at least one node upstream of the grounding line are deactivated. Clipping the ocean mesh may result in some elements along the boundary which are only connected by one edge to the rest of the domain. No circulation can pass through these elements and they are also deactivated. Consequently, FESOM elements will always remain downstream of the communicated grounding line position (see Fig. 2c).

Subsequently, the three-dimensional FESOM mesh is derived from the updated ice shelf draft and the constant ocean bathymetry. The ice draft in Úa is interpolated to the FESOM node locations using the linear method in Cartesian space. The calving front in FESOM is determined by the boundary of the Úa domain and Úa ice thickness. Where the Úa ice draft solution is smaller than half the thickness of the uppermost layer in FESOM, the draft is rounded to zero and no ice shelf will be present at the respective FESOM grid node. We note that these manipulations do not systematically smooth the vertical calving face and, thus, do not support spurious surface water intrusions (see Malyarenko et al., 2019, for a discussion on the representation of processes near the ice front in ocean models). For the simulations presented in this study, the minimum ice thickness in Úa is at least half the thickness of the uppermost layer in FESOM and, consequently, calving front positions are always identical between the models. Further, the FESOM numerics require a minimum water column thickness of two layers and a minimum overlap between adjacent water columns of at least two layers. Both of these conditions are ensured by artificial deepening of the sea floor if necessary, an established option for ice shelf-ocean simulations with FESOM (Schnaase and Timmermann, 2019). We note that these manipulations are reset at each subsequent coupling step and are not communicated to the ice model (other than possibly through the melt rates).

After the three-dimensional FESOM mesh is established, ocean conditions in new cavity regions must be initialised. Water columns are added where the grounding line has retreated or/and extended upward where the ice shelf has thinned. Sea surface height (ssh) of new water columns is derived from the nearest neighbour in Cartesian space, so that ssh gradients in newly ungrounded regions are small. The three-dimensional temperature and salinity fields are first extrapolated horizontally and then vertically using the nearest-neighbour approach. All velocities in all new ocean cells are initially set to zero. We note that this approach is not strictly conservative, but we expect the flushing time of new regions to be orders of magnitude smaller compared to the smallest possible coupling interval (monthly).

2.6 Model configuration

Important aspects of our modelling choices are summarised in Table 1. The idealised setup used in this study is referred to as the research-group-typical (TYP) configuration in the MISOMIP1 terminology, with most aspects being consistent with the pan-
160 Antarctic case. In both cases, for example, englacial stresses are modelled using the Shallow Shelf Approximation and Glen's flow law while basal sliding is parameterized using the Weertman sliding law. A minimum ice thickness of 10 m is enforced in both setups. For the idealised case, however, this is achieved using the active-set method, whereas for the realistic case, we reset the thickness field outside the Newton-Raphson step (deactivated the active-set method), to resolve convergence issues in regions of thin, fast flowing ice near rock outcrops. We note that none of these choices are hardwired into the framework and
165 they can all be modified by the user. For example, Úa has about 5 different sliding laws implemented and the active-set method can also be used for realistic cases.

	Idealised	Realistic
Úa		
Horizontal resolution	8 km to 2 km	180 km to 2 km
GL refinement (distance in km: refinement in km)	(20: 5, 5: 2)	(20: 10; 10: 8; 8: 6; 6: 4; 4: 3; 3: 2)
Basal traction	Weertman (m = 3)	Weertman (m = 3)
Englacial stresses	SSA, Glen's law	SSA, Glen's law
	(n = 3, A = 2.0 x 10^{-8} kPa^{-3}a^{-1})	(n = 3, A = 2.0 × 10^{-8} kPa^{-3}a^{-1})
Minimum ice thickness	10 m	10 m
Thickness constraint	Active-set method (mass conserving)	Not mass conserving
FESOM		
Horizontal resolution	2 km	340 km to 2 km
Number of levels for vertical coordinate	36	100
Vertical resolution in sub-ice shelf cavity	20 m	10 m to 30 m
Horizontal background viscosity	100 m^{2}s^{-1}	Scaled with resolution
		(100 m^{2}s^{-1} where 2 km)
Horizontal diffusivity	10 m^{2}s^{-1}	Scaled with resolution
		(10 m^{2}s^{-1} where 2 km)
Vertical mixing	kpp	kpp
Equation of state	Non-linear	Non-linear
Minimum ice thickness	10 m	10 m
Coupler		
Coupling interval	1 year (also 1 month)	1 year

Table 1. Selected modelling and parameter choices for Úa, FESOM and the coupler for the idealised and realistic test cases.

In FESOM, ice shelf basal melting and respective heat and virtual freshwater fluxes are modelled using the 3-Equation melt parameterisation (Hellmer and Olbers, 1989) with velocity-dependent boundary layer exchange coefficients for heat and salt (Holland and Jenkins, 1999). Following the MISOMIP1 protocol we compute thermal driving in potential temperature space and include a background tidal velocity of 0.01 m/s. The inputs for the melt parameterisation, that is mixed layer velocity, salinity and temperature, are derived by averaging between the uppermost two vertical coordinate levels in FESOM (i.e. using the mean over the uppermost layer). Heat and virtual freshwater fluxes enter the ocean model's computational domain as boundary conditions applied at the surface. Melt rates calculated along the FESOM grounding line are of particular importance, as they determine the basal mass balance in the grounding zone of the ice model to a large degree. We choose a free-slip momentum boundary condition for FESOM's boundary nodes within ice shelves cavities to facilitate the computation of velocities (and consequently melt rates) along the cavities' perimeters.

The coupling interval chosen for both the idealised and the pan-Antarctic application is one year. Additionally, we have performed an idealised experiment with monthly coupling to investigate the sensitivity of our results to the coupling frequency.

3   Evaluation using the MISOMIP1 framework

3.1   Experimental design

The Marine Ice Sheet Ocean Model Intercomparison Project phase 1 (MISOMIP1) provides a framework to test and compare the behaviour of coupled models using a set of idealised and well constrained experiments. The protocol is provided by Asay-Davis et al. (2016) and we use the IceOcean1ra (retreat and advance without dynamic calving) experiment to test fundamental aspects of our model, such as numerical stability, plausibility of the ice draft and grounding line evolution, and the magnitude of inaccuracies in mass, salt and heat conservation. We note that future studies aiming to implement variable calving front positions in Úa-FESOM should use the IceOcean2ra experiment. Úa-FESOM results have been provided to the working group of MISOMIP1 and will be included in the comparison.

The initial configuration for the IceOcean1ra experiment is a steady state, marine terminating ice sheet, buttressed by a confined ice shelf and exhibiting a grounding line that rests on a retrograde part of the bed slope. We have derived this configuration in a 20,000 year Úa standalone simulation with no ice shelf basal melting. The ocean is initialised for the final ice-sheet geometry with uniform surface freezing point temperature and a salinity profile that provides a stable stratification (linearly distributed from 34.55 at depth to 33.80 at the surface). During the first 100 years of the coupled experiment, the far-field ocean is warmed instantaneously with a temperature profile reaching 1 °C at depth, intended to cause ice shelf thinning and grounding line retreat. Subsequently, cold ocean conditions are restored and the glacier is expected to re-advance to some degree within the second 100 years of the simulation.

3.2 Computational mesh

Figure 2a shows Úa's mesh at the beginning of the coupled simulation. The background mesh features a uniform resolution of 8 km and has been derived using the mesh2d routines (Engwirda, 2014). This mesh is augmented by local adaptive mesh refinement and coarsening around the grounding line with up to 2 km resolution using the newest vertex bisection method (see Mitchell, 2016).

The two-dimensional extended ocean mesh covers the entire ocean and ice sheet domain using a uniform resolution of 2 km and has been derived using the jigsaw algorithm (Engwirda, 2017). As described above, elements of this mesh are deactivated according to Úa's grounding line position and Figure 2b shows the clipped configuration at the beginning of the run. In the vertical dimension we use 36 equally spaced levels with 20 m layer thickness.

3.3 Results and Evaluation

Over the course of the MISOMIP1 retreat and readvance simulations, FESOM is numerically stable and Úa exhibits fast convergence behaviour. Restarting FESOM with an extended cavity and updating the basal mass balance in Úa can pose challenges for the numerical solvers. The simulation comprises a reasonable test for the numerical solvers as the IceOcean1ra experiment produces rapid glacier retreat (0.2 km/yr, not shown) forced by high basal melt rates (50 m/yr), which are conditions reminiscent of certain areas in West Antarctica. Further, differences between restarts increase with the length of the coupling interval, adding more stress on the numerics of the models, and we consider 12 months to be a rather long coupling interval (c.f. Asay-Davis et al., 2021). Úa converges in less than 6 Newton-Raphson iterations with time steps between 0.025 and 0.1 years, resulting in less than 2 minutes walltime per model year. FESOM runs with a constant timestep of 12 minutes and takes 22 minutes walltime for one year model time when deployed on 192 CPUs.

The simulated ice sheet retreat and readvance behaviour follows the variations in ocean thermal forcing. Figure 3 shows snapshots of cavity shape, ocean temperature and melt rates, and Figure 4 presents the evolution of integrated ocean and ice quantities. Increasing ocean thermal heat at the northern boundary causes ice shelf thinning, grounding line retreat and acceleration of grounded ice mass loss. During the second half of the experiment, when the heat source is removed, ice shelf shape and grounding line position recover in part and the rate at which sea-level-relevant ice is lost slows down.

Melting up to 50 m/yr in the deep parts of the cavity is consistent with the ocean thermal forcing of about 2 °C (Fig. 3). Some differences between the evolution of the total meltwater flux (Fig. 4eg) and the signal of the mean ocean temperature (Fig. 4ge) are expected and a result of the evolving cavity geometry. The high-frequency variability in the melt signal during the retreat period can be explained by its direct coupling to changes in buoyant plume strength caused by updating the ice base slope. The slow decrease in melt flux between year 10 and 100, despite temperatures being constant, is caused by an overall steepening of the ice shelf slope towards the grounding line, which shifts larger parts of the deep-drafted ice shelf areas into
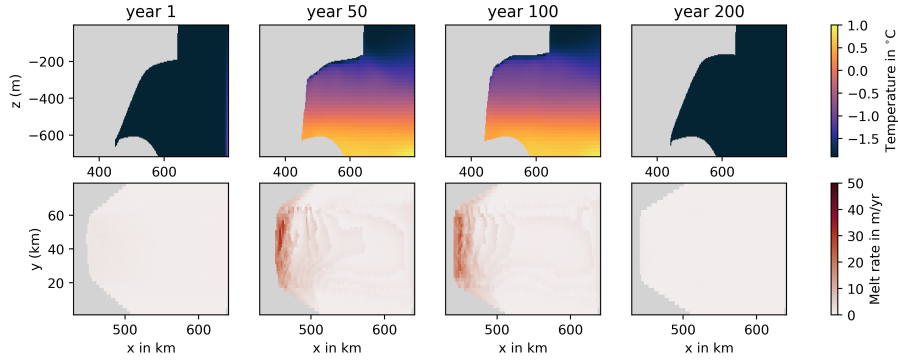
Figure 3. Snapshots from the idealised experiment. Top row: side view of ice draft geometry and ocean temperature at the centerline at different times. Bottom row: top-view of corresponding melt rates.

colder waters.

The mean ocean salinity evolution (Fig. 4f) is a result of two competing sources. The ocean forcing includes salinification at
235 the northern boundary (to obtain the same density profile with the increased temperature), which explains the initial increase in salinity in the domain. Glacial melt water freshens the ocean and after a few years this offsets the forcing signal. Bulk salinity approximately equilibrates, and small-amplitude temporal variations track changes in basal meltwater production. After 100 years the cold and fresh ocean conditions are instantaneously restored at the northern boundary, causing a distinct drop in salinity, before melting ceases as well and salinity recovers to some degree.

240

Conservation inaccuracies are small compared to the forcing signal. No sea level adjustments had to be applied, as FESOM incorporates the meltwater as a virtual salinity flux, while the ocean volume changes only according to the change in cavity geometry (adjustments are recommended for other approaches, see Asay-Davis et al., 2016). Nevertheless, Úa-FESOM is not strictly mass conserving locally, as different grounding line definitions are used in the ice and ocean components and melt rates
245 are interpolated between grids (described above). Inconsistencies arise from the temporal lags between updating melt rates in Úa and cavity geometry in FESOM and from interpolating the communicated quantities between different grids and masks using non-conservative methods (also see Gladstone et al., 2021). We calculate mass conservation deviations using the virtual freshwater salinity flux in FESOM and the basal mass balance in Úa. We find that differences in total mass flux at any given time of the experiment are an order of magnitude smaller compared to the forcing signal (Fig. 4g). More ice mass is lost in the
250 ice model than gained in the ocean model and this discrepancy accumulates to about 3% of the total mass lost at the end of the experiment (Fig. 4h). This number could potentially be reduced in future studies Currently, Úa's grounding zone extends into regions slightly upstream of FESOM's grounding line and melt rates are extrapolated into these regions (see Sec. 2.4). We expect this issue to explain most of the discrepancy in mass flux. Future studies could potentially improve the behaviour by tuning the grounding line definition used in the Úa-to-FESOM step, that is choosing a value smaller than 0.5 to define the
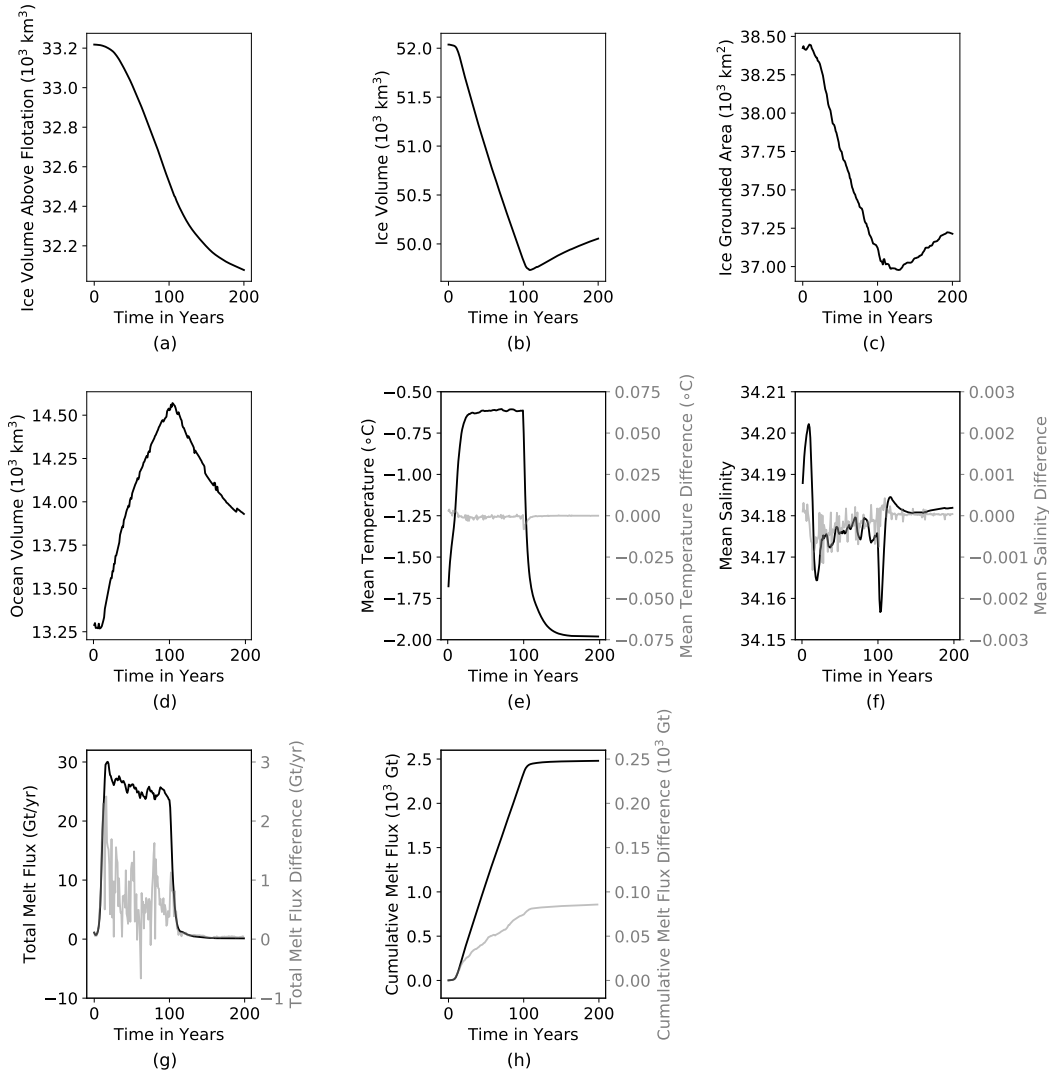
Figure 4. Evolution of integrated quantities of the idealised experiment. (a) total ice volume, (b) total ice volume above flotation, (c) change in grounded ice area, (d) total ocean volume, (e) mean ocean temperature, (f) mean ocean salinity, (g) total melt water flux from the ice model and (h) cumulative total melt water flux from the ice model. Panels (e) to (h) also present the inaccuracies of the respective quantities due to the coupling (grey lines, axes on the right sides) with axis ranges scaled up by a factor of ten compared to the absolute values (black lines, axes on the left sides). Positive differences in (g) and (h) describe additional mass loss from the ice model compared to the mass gain in the ocean model.

255 grounding line in Úa's grounding/floating mask.
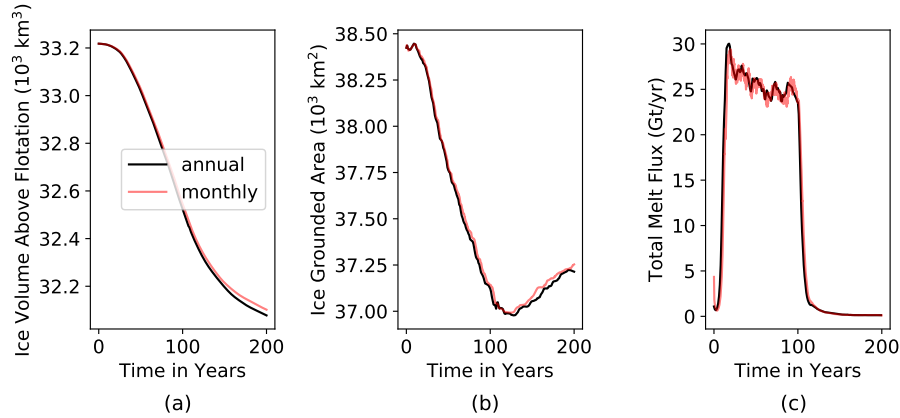
Figure 5. The effect of reducing the coupling interval. Evolution of (a) ice volume above flotation, (b) ice grounded area and (c) total melt water flux for annual and monthly coupling.

Extrapolation of ocean hydrography into new cavity regions after each FESOM-to-Úa coupling step potentially introduces an artificial heat or freshwater source. We quantify the impact of this effect by comparing the domain-average salinity and temperature at the beginning of a coupling period to the final state of the previous coupling period (Fig. 4e and 4ff and 4e).
260 These inaccuracies are two orders of magnitude smaller compared to variations from the forcing.

As mentioned above, inaccuracies grow with the length of the coupling interval, potentially leading to substantially different results. Figure 5 shows the sensitivity of our results to increasing the coupling frequency from annual to monthly. Grounded ice mass loss decreases by about 2% of the forcing signal and differences in the grounded area and total melt water flux are
265 even smaller. These results validate our sequential approach and show that annual coupling is appropriate for this particular experiment. Further, as the IceOcean1ra experiment resembles some of the most rapidly changing ice sheet-ocean systems observed around Antarctica, our results also suggest that faster-than-annual coupling is an unnecessary use of computational resources to investigate centennial-scale ice sheet evolution. Generally, the optimal coupling frequency will need to be decided on a case-by-case basis and will not only depend on the numerics (e.g. fast retreat might require shorter coupling timesteps to
270 avoid large step-functions in geometry), but also the research question and its related timescales of interest.

4   Application to the pan-Antarctic domain

4.1   Experimental design

To showcase Úa-FESOM, we perform global ocean/pan-Antarctic Ice Sheet simulations for the historical period 1979-2018. Figure 6 outlines our procedure to prepare and perform the experiment. After inversion, the ice model is stepped forward in
275 time for 20 years using constant ice shelf basal melt rates from FESOM's spin-up (see below, the mean of the last 5 years).
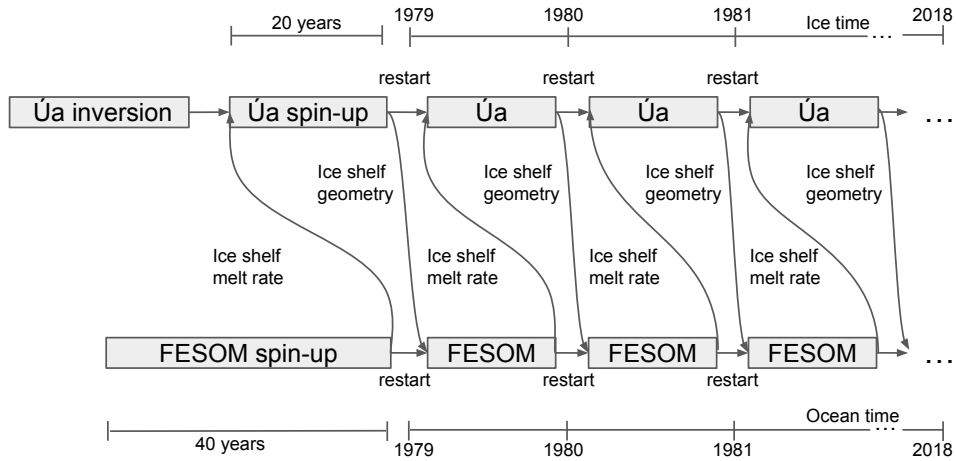
Figure 6. Realistic test case experimental design. After inversion, the ice model is allowed to relax for 20 years using constant melt rates from an equilibrated ocean before melt rates are updated every year for the historical period 1979-2018.

During this relaxation period ice dynamics adjust to inconsistencies between inversion inputs and forcing. Ice shelf basal melt rates and cavity geometry are then updated at an annual interval to simulate the target period of 39 years.

An ice sheet inversion is performed for the rate factor and basal slipperiness distribution using the ice sheet geometry data from Bedmachine (Morlighem et al., 2020) and observed surface velocities from the MEaSUREs project, following an adjoint method (MacAyeal, 1993). The ice sheet surface mass balance is a mean for the simulation period derived from RACMO2 (Van Wessem et al., 2018). Calving front positions are constant and determined by the initial geometry.

FESOM's initial mesh geometry is obtained from the global bathymetry data from RTopo-2 (Schaffer et al., 2016) and Úa's initial ice draft, which is based on Bedmachine (Morlighem et al., 2020). The ocean is initiated at rest and using the hydrography from the World Ocean Atlas (WOA18). Temperature and salinity are extrapolated into the sub-ice shelf cavities. The surface of the ocean/sea-ice is forced with output from the ERA-Interim atmospheric reanalysis (Dee et al., 2011) updated at daily intervals. We use one forcing cycle from 1979-2018 as ocean spin-up and repeat this cycle during the coupled simulation.

4.2 Computational mesh

In contrast to the idealised case, Úa's ice draft depth and grounded/floating mask is not directly interpolated onto the extended FESOM mesh, but combined with the RTopo-2 ocean bathymetry first (see Fig. 1). We use RTopo-2 at 1 min resolution, which is everywhere finer than our FESOM mesh, and perform interpolation using the linear method. The three-dimensional FESOM mesh is then derived from the global data following the procedure described in Section 2.5.

Figure 7 presents the mesh horizontal resolution in the ocean and ice models at the beginning of the transient run. FESOM's resolution varies from 340 km in the deep ocean to less than 10 km inside the sub-ice shelf cavities (Fig. 7a and 7b). The
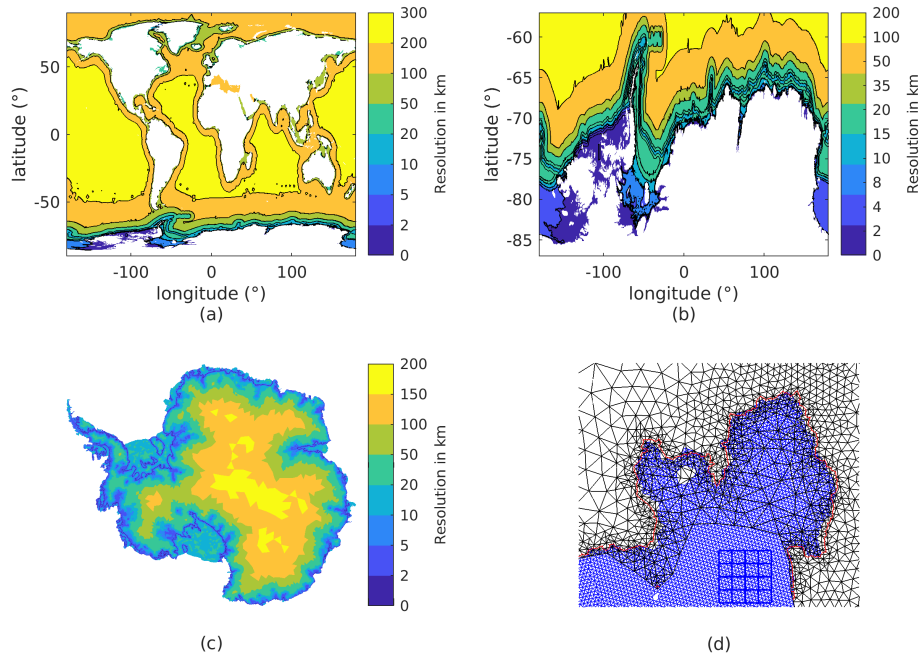
Figure 7. Horizontal mesh resolution for the realistic experiment. (a/b) FESOM's global mesh is refined around the Antarctic continental shelf with up to 2 km grid spacing and extends into regions which could possibly unground during the course of the simulation. (c) Úa's mesh is refined in regions of high strain rates and grounding lines are tracked with 2 km resolution. (d) Detail showing initial ice mesh (black), ocean mesh (blue) and grounding line location (red) for Pine Island Ice Shelf. Blue box visualises the resolution of a quarter-degree ocean model (about 7.3 km at 74.8° S).

295   background mesh extends into regions which would unground if Úa's ice thickness were instantaneously reduced by 50%. Initial grounding zones and all potentially ungrounding regions are covered with 2 km resolution. In the vertical, the ocean is discretized into 100 levels, with increased resolution in the upper ocean. Within the sub-ice shelf cavities, the layer thickness ranges from 10 to 30 m. Úa's background mesh features coarse cells with up to 180 km resolution in the ice sheet interior and refinement of up to 4 km resolution in regions of high strain rate, e.g. near ice stream shear margins (Fig. 7c). Adaptive mesh

300   refinement down to 2 km resolution is included during the relaxation and coupling period.

The advanced mesh flexibility in the ice and ocean model played a critical role during the development stage. Figure 8 shows the ocean conditions in the Amundsen-Bellingshausen Seas for different FESOM configurations. An initial mesh featured resolutions between 5 km and 50 km on the continental shelf outside the ice shelf cavities. This set-up resulted in a

305   poor representation of warm deep water intrusions, which are known to control ice shelf melting in this region (e.g. Pritchard et al., 2012). Increasing the resolution to 2 km over the entire continental shelf of the Amundsen-Bellingshausen Seas drastically improved the representation of warm deep water intrusions onto and across the continental shelf. Raising the the drag coefficient at the ice shelf base (C_d), involved in the calculation of momentum and the turbulent exchange of heat and salt
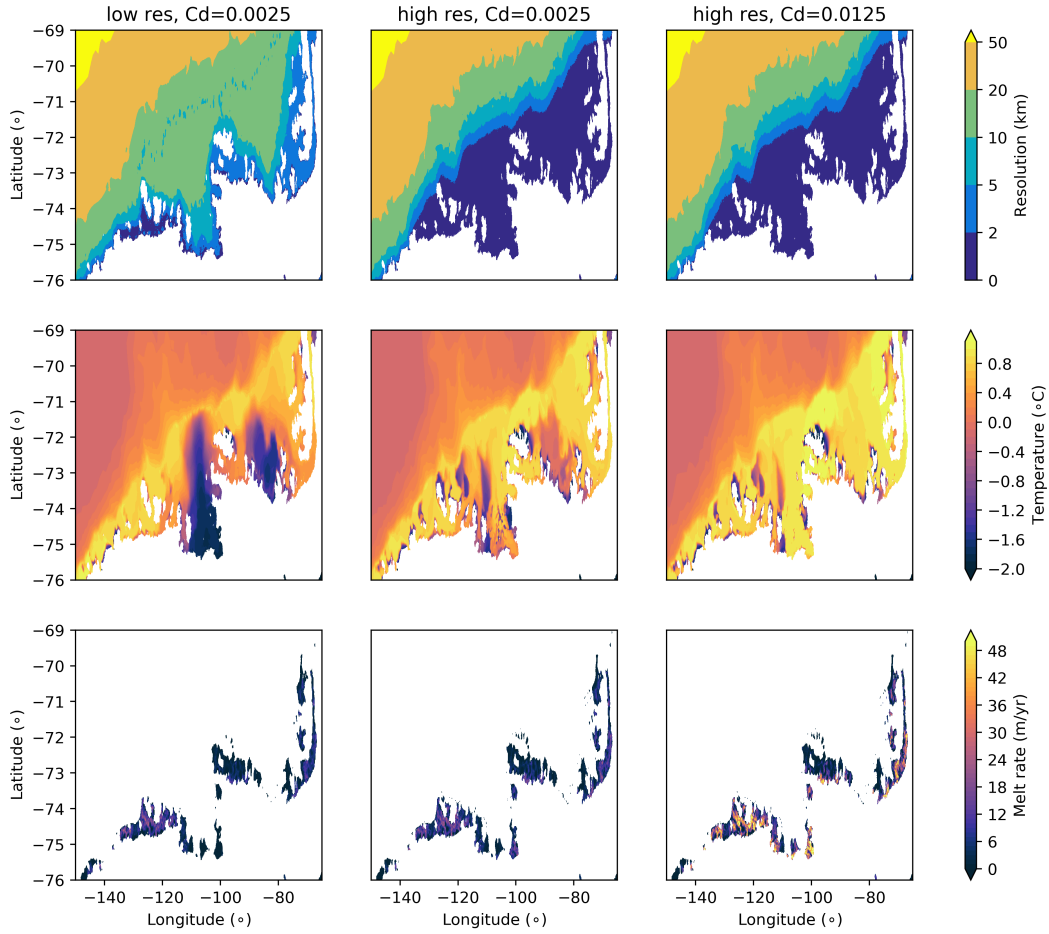
Figure 8. Simulated ocean conditions in the Amundsen-Bellingshausen Seas in three FESOM experiments with different resolutions and turbulent exchange coefficients. Horizontal resolution in the ocean model (top row), annual mean bottom layer temperature (middle row) and ice shelf melt rates (bottom row) at the end of the spin-up. Increasing the resolution from about 10 km (left column) to 2 km (middle column) drastically improves the representation of deep warm water intrusions across the shelf break. Raising the drag/turbulent exchange coefficient (C_d, right column) further increases ice shelf melting and strengthens the circulation of the warm water towards the ice sheet grounding lines.

through the ice-ocean boundary layer (see Holland and Jenkins, 1999), further increased ice shelf melting and strengthened the circulation of the warm water towards the ice sheet grounding lines. Increasing horizontal resolution and tuning of C_d are established approaches to derive realistic conditions in this difficult-to-model region (Nakayama et al., 2014, 2017). Note that C_d=0.0025 is not part of the coupled perturbation experiment but only used during the development of the ocean model spin-up.
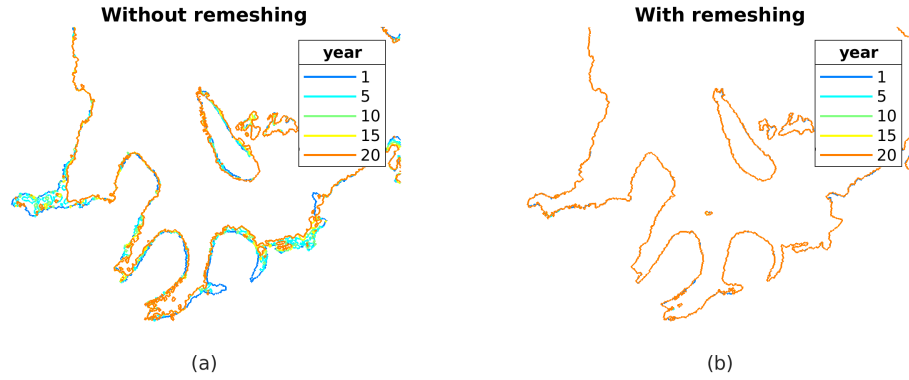
Figure 9. Grounding line evolution with and without adaptive remeshing in Úa. Grounding line positions at different times of the relaxation period when refining the mesh once based on the initial position of the grounding line (a) and including mesh refinement around grounding lines (and coarsening away from grounding lines) at every timestep (b). Adaptive remeshing is necessary to maintain realistic grounding line positions.

Similarly, without Úa's adaptive remeshing, that is using a mesh which is refined around the initial position of the grounding lines but does not change throughout the simulation, glacier evolution is unrealistic in some regions. We find this behaviour to be most pronounced during the relaxation period and in cold regions, where ice streams drain into cavity parts with shallow water column thickness. Figure 9 shows this effect for the Filchner Ronne Ice Shelf.

4.3 Results

It is a particular challenge for large-scale coupled models to accurately predict the grounding line evolution of the rapidly retreating glaciers in West-Antarctica. Siahaan et al. (2022), for example, report an unrealistic grounding line advance of Pine Island and Thwaites Glacier in their Earth System Model simulations of the coming century. Their ocean component has a $1°$ horizontal resolution, which results in an order of magnitude lower spatial resolution in Pine Island Bay compared to our Úa-FESOM configuration (see Fig. 7d).

We use the turbulent exchange coefficient at the ice shelf base (C_d) to calibrate the evolution of the grounding line of Pine Island Glacier. C_d is a typical tuning parameter for ice shelf melting in ocean models (see, e.g., Nakayama et al., 2017) and, thus, should impact the evolution of glacier systems controlled by ice-ocean interaction. We expect particular sensitivity for Pine Island Glacier, as it is known for rapid retreat behaviour triggered by ocean-induced melt (Rignot et al., 2014; De Rydt et al., 2021).

Figure 10 shows the sensitivity towards the choice of C_d in ice shelf basal melting, the ice thickness trend and the evolution of the grounding line of Pine Island Glacier. Predicted melt rates for $C_d = 0.0125$ frequently exceed 50 m/yr in the Pine
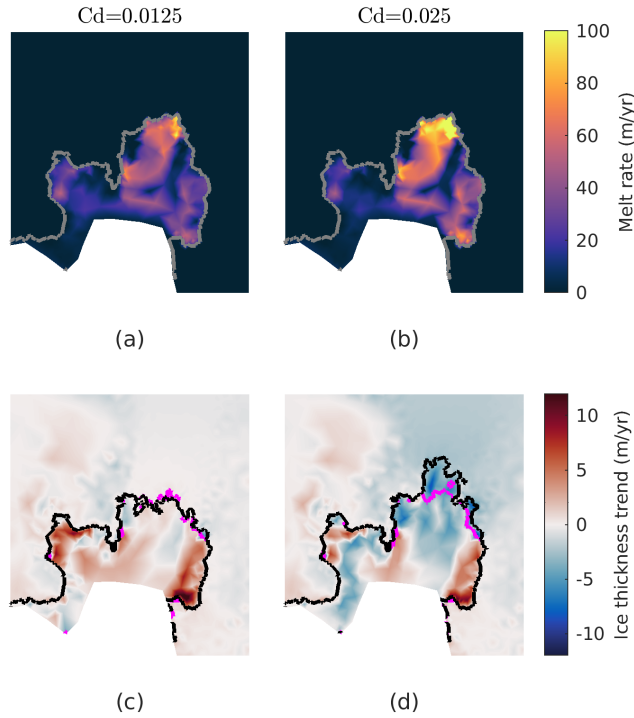
Figure 10. Pine Island Glacier response to variations in C_d. For C_d=0.0125 and C_d=0.025: (a, b) ice shelf melting at the beginning of the coupled simulation, (c, d) mean change in ice thickness during the 39 years of the coupled experiment. In (c) and (d), positive values (red) depict ice thickening and grounding line positions at the start and end of the coupled simulation are shown in magenta and black, respectively.

Island Ice Shelf grounding zone (Fig. 10a). Increasing C_d to 0.025 results in melting with a similar pattern, but substantially
335 elevated magnitude (Fig. 10b). Grounding line melt is now on the order of 100 m/yr, which compares well with observations
by Dutrieux et al. (2013) and Shean et al. (2018). In both cases, the grounding line advances during Úa's relaxation period to
similar positions. During the 39 years of coupled simulation, the smaller C_d value results in moderate ice thickness changes in
the grounding zone (mostly less than 2 m/yr) and a stable grounding line position (Fig. 10c). For the higher C_d value, ice shelf
thinning exceeds 5 m/yr in many regions near the grounding zone and the grounding line retreats by tens of kilometres (Fig.
340 10d). Consistent with the grounding line retreat behaviour, the drainage basin of Pine Island Glacier loses more mass for the
higher C_d case, now clearly reproducing the observed trend (Smith et al., 2020).

The model's behaviour in other regions is consistent with observations in many aspects, though it also shows some dis-
crepancies. Figure 11 presents results for the Filchner-Ronne Ice Shelf (FRIS) and the Totten-Moscow University ice shelf
345 system. The pattern and magnitude of melting and refreezing underneath FRIS (Fig. 11a) are typical for cold water ice shelves
and compare well with satellite-derived estimates (e.g. Adusumilli et al., 2020). However, glaciers draining into FRIS exhibit
spurious oscillations in ice thickness evolution (Fig. 11b). The (unrealistic) changes in ice thickness are widespread, but mostly
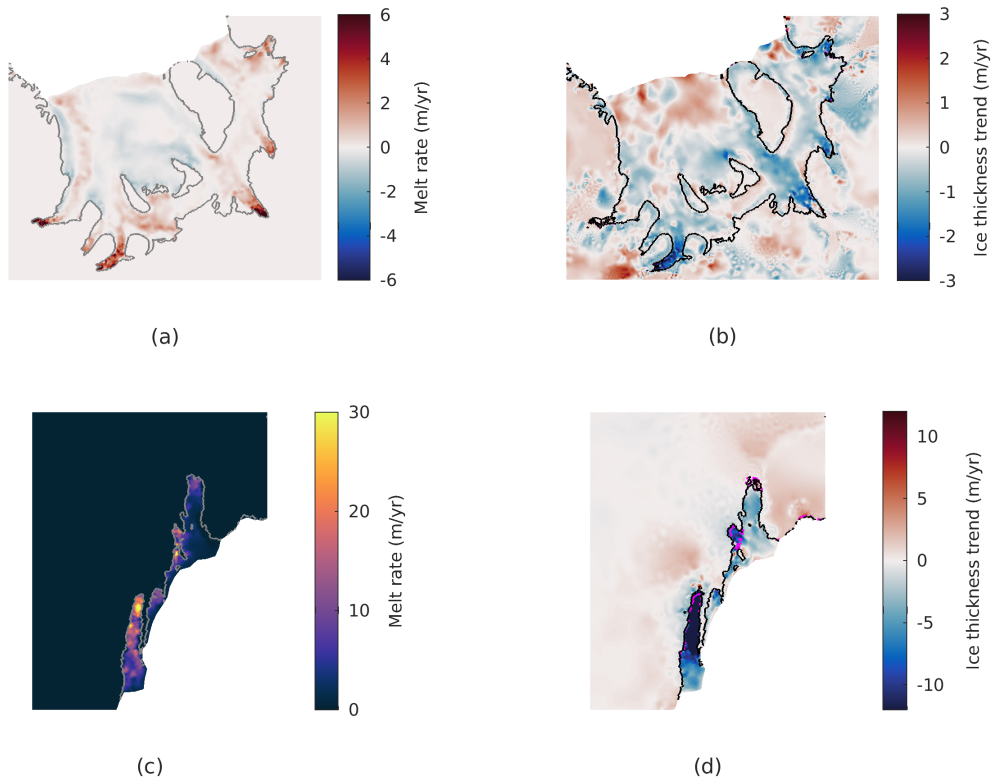
Figure 11. Coupled model results for the regions around (a/b) Filchner-Ronne Ice Shelf and (c/d) the Totten-Moscow University ice shelf system. Ice shelf melting at the beginning of the coupled simulation (a and c) and mean change in ice thickness during the 39 years of the coupled experiment (b and d). In (b) and (d), positive values (red) depict ice thickening and grounding line positions at the start and end of the coupled simulation are shown in magenta and black, respectively. Results are taken from the simulation with C_d=0.0125.

confined to grounded ice upstream of the refined mesh near the ice shelves. Further, warm deep water intrusions outside the Amundsen-Bellingshausen Seas are not necessarily well represented. For Totten glacier, for example, the model underestimates ice shelf melting near the grounding line (Fig. 11c) and, consequently, grounded ice thinning (Fig. 11d).

The biases described above are specific to the configurations of Úa or FESOM and can likely be addressed through improvements to the individual components or their setup. For instance, various approaches to suppress spurious elevation changes in Úa have been followed, such as longer spin-up times (Naughten et al., 2021; De Rydt and Naughten, 2024) and/or the addition of changes in ice thickness to the cost function in the inversion (De Rydt and Naughten, 2024). Similarly, biases in warm deep water intrusions require careful investigation from the ocean modeling perspective. A recent study by Hirano et al. (2023) highlights the role of deep bathymetry troughs, not accounted for in our model, in facilitating deep warm water intrusions near Totten Glacier. Furthermore, horizontal ocean resolution should be locally calibrated — similar to the efforts for Pine Island
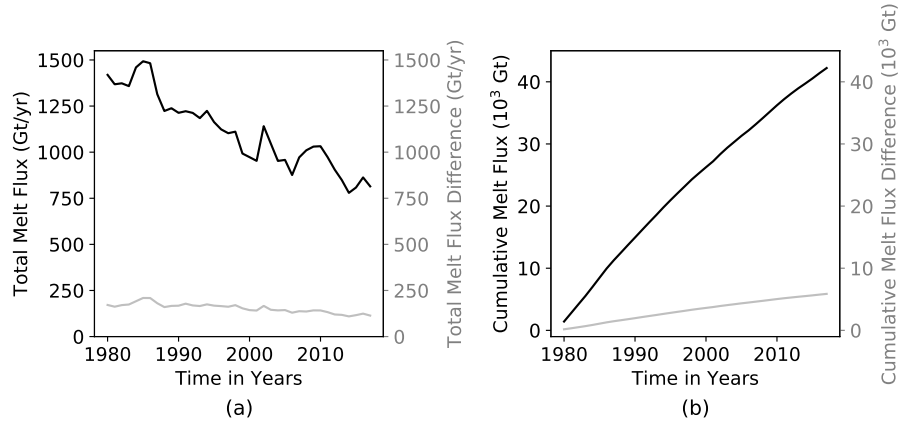
Figure 12. Antarctic melt water flux. (a) shows total melt water flux from the ice model (black, axis on the left side) and its difference to the flux calculated by the ocean model (grey, axis on the right side). (b) shows the cumulative sums of the flux and the inaccuracy. Differences are presented using the same scale as the absolute values, with positive differences indicating additional mass loss from the ice model relative to the mass gain in the ocean model.

Glacier — to ensure an accurate representation of the oceanic processes involved in deep warm water transport.

360

Discrepancies in the melt water flux between Úa and FESOM are considerably larger for the realistic experiment. Figure 12 shows the evolution of the Antarctic-wide ice shelf melt water flux as calculated by Úa and how this differs to the melt-water gain calculated by FESOM. The ice model loses about 16% more freshwater than FESOM gains and this inaccuracy accumulates to about 6,000 Gt during the course of the simulation. In the idealised experiment, small discrepancies are caused

365 by differences in grids and masks between Úa and FESOM. The increased complexity of realistic ice shelf configurations, however, have exacerbated the issue. A closer match between Úa's and FESOM's melt rates can be achieved with further 'fine tuning' of the gridding and interpolation algorithms (see suggestions for the idealised case). As this tuning is case-dependent, however, it is not the focus of this study. Finally, we note that it remains to be shown how biases and uncertainties in the ice-ocean coupling impact the dynamics of the system, compared to other missing or poorly represented processes, such as

370 calving and subglacial discharge.

While a fully optimized, calibrated and tested setup for Antarctica is beyond the scope of this study, we have demonstrated some key improvements for the pan-Antarctic domain compared to previous approaches. These advancements provide a strong foundation for future calibration and validation efforts. Future improvements to the individual model components will be

375 integrated into the coupled setup.

4.4 Performance

For our global ocean/pan-Antarctic test case, we run FESOM on an NHR computer using 3840 CPUs, Úa on the AWI supercomputer Albedo using 6 CPUs and the coupling routines on an AWI desktop machine using 1 CPU (also see Sec. 2.3). This set-up requires about 13 days walltime (without queuing time on the supercomputer), 200 000 core-h and 1.2 TB storage space for 39 years of coupled simulation with annual coupling time step. Figure 13 compares the demands of the individual components for one coupling cycle (one year of model time). The ocean mesh comprises two orders of magnitude more elements than the ice mesh (54 million compared to 250 thousand) and FESOM's computational demand exceeds Úa's by about the same ratio. Most of the wall time is used by our configuration of the ice model, which is not massively parallelized. The coupling routines account for approximately 20% of the overall wall time and storage needs, with most of these demands stemming from the Úa-to-FESOM step. We note that the comparison between Úa and FESOM is influenced not only by the level of parallelization but also by the varying hardware environments. Nonetheless, we anticipate that future studies will benefit from this assessment for rough estimations of resource requirements.

A parallel coupling approach could substantially improve the performance. We have chosen a sequential approach based on the assumption that the wall time of the ocean and ice model step roughly scales with their computational demands. This assumption turned out not to be true, as Úa has not been designed to run in massively parallel mode. Future studies could avoid the walltime of the faster component (here the ocean model with 33%) by adapting the coupler to run the ice and ocean model step in parallel (as, e.g., done for Úa-MITGCM, Naughten et al., 2021).

Within the Úa-to-FESOM step, a full three-dimensional ocean mesh is generated, accounting for 92 % of the coupler's walltime and limiting the coupling frequency for large applications. A wetting and drying scheme within FESOM would open a path to reduce this overhead. Goldberg et al. (2018) has adapted the wetting and drying scheme of their ocean model to allow for cell activation within ice shelf cavities. Together with vertical remeshing (see Jordan et al., 2018), this would allow to establish a three-dimensional background mesh which is constant throughout the coupled simulation. Although realistic bathymetries and the unstructured meshing approach of FESOM pose further challenges, this might be a promising path to pursue for future studies that aim to improve the coupler's performance.

5 Summary and Conclusions

We have presented a new framework to couple the ice sheet model Úa and the ocean model FESOM. The framework uses a sequential approach to communicate ice shelf basal melt rates and ice draft geometry using simple interpolation techniques. The coupling step is independent of the forward time-steps of the ocean and the ice-flow model and can be chosen at a multiple of monthly intervals. New cavity regions are initiated with hydrographic properties from the nearest wet cell in cartesian space, and with zero momentum.

We have evaluated the code using an idealised grounding-line retreat and readvance experiment. The model is stable with an annual coupling interval and ice draft thinning and thickening as well as grounding line retreat and advance are consistent
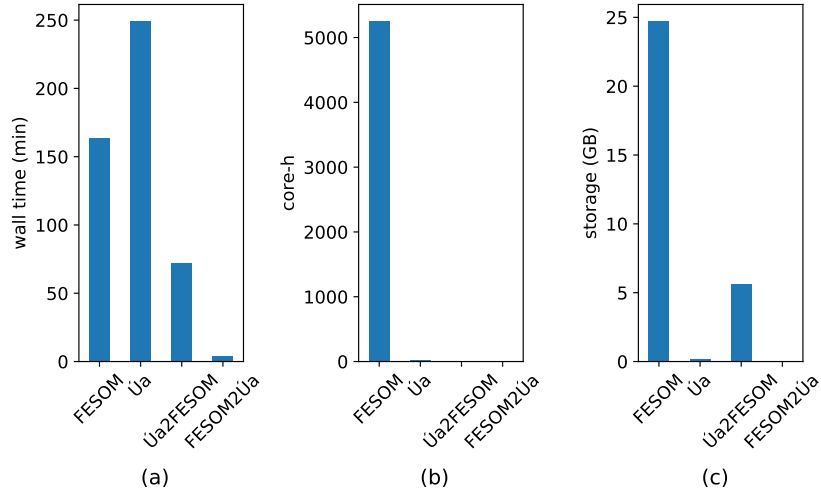
Figure 13. Resource requirements of the pan-Antarctic test case using our infrastructure. (a) walltime, (b) core hours and (c) storage space needed for the individual components of the coupling cycle to simulate one year of model time. Úa uses adaptive time stepping and presented quantities are mean values. Our FESOM set-up uses most of the computational resources but is highly parallelised (3840 CPUs) and, thus, faster than our Úa set-up (6 CPUs). Both coupling routines together take about half the time of the 1-yr ocean model run. Due to the fact that a FESOM mesh needs to be newly generated for each coupling step, the Úa-to-FESOM step (denoted as Úa2FESOM in the panels)) requires much more time than FESOM-to-Úa (denoted as FESOM2Úa).

with the ocean forcing. Remapping of the ocean state causes differences in mean ocean salinity and temperature that are orders
410 of magnitude smaller compared to the forcing signal. The ice sheet loses more mass than the ocean gains due to differences in the definition of the grounding line and the leak accumulates to 3% of the total mass loss at the end of the 200-yr experiment. Reducing the coupling interval from annual to monthly changes grounded ice mass loss by 2% compared to the forcing signal. These results suggest that the sequential approach and an annual coupling interval are sufficiently accurate to predict ice sheet evolution over centennial timescales.

415

Further, we have demonstrated the capabilities of our model by simulating 39 years of historical Antarctic-global ocean interaction. We used an annual coupling interval and spatial resolutions of the ice and ocean domains previously only applied to regional studies. Ocean model tuning leads to Pine Island Glacier retreat consistent with observations, which is a known challenge for coarser-resolution models due to its dynamic grounding line behaviour and susceptibility to ocean changes un-
420 derneath its small and entrenched ice shelf. Model biases are specific to the ice or ocean component and can be addressed through updates and careful initialization and calibration.

We conclude that the framework is well suited to answer scientific questions regarding Antarctic ice sheet-ocean interaction over centennial timescales. The realistic test case presented here demonstrates the ability of Úa-FESOM to capture important

425 information about small-length scale ice-ocean processes and feedbacks that are critical to improve projections of the Antarctic contribution to sea level rise. This is in particular due to its unique capability to locally refine and adapt the horizontal mesh resolution of both model components, whilst keeping computational costs viable.

Code availability. The exact versions of Úa, FESOM and the coupler used to produce the results for this paper are archived on Zenodo (Richter, 2024). The archive also includes the input files to run Úa and FESOM in their coupled and standalone configuration, the scripts
430 to set up new coupled experiments and to produce the plots. The maintained version of Úa (https://github.com/GHilmarG/UaSource) is available at github, while the maintained version of the coupler and FESOM-1.4 will be available from the authors upon request. Datasets used to run the realistic application are stated and referenced in the text.

Author contributions. OR developed the coupler, set up FESOM and Úa, designed and conducted the experiments and prepared the manuscript. RT contributed to the development of the coupler and the set-up of FESOM, advised on the design of the experiments and contributed to the
435 writing of the paper. HG and JDR contributed to the Úa configurations, advised on the development of the coupler and experimental designs and contributed to writing the paper.

Competing interests. The authors declare that they have no conflict of interest.

Acknowledgements. We would like to thank Verena Haid, Emily Hill and Claudia Wekerle for contributions to the code and helpful discussions; Wolfgang Cohrs, Natalja Rakowsky, Malte Thoma, and Sven Harig for maintaining excellent computing facilities at AWI. We
440 thank the Nationales Hochleistungsrechnen (NHR) alliance for providing computer resources through project hbk00097. This publication was supported by PROTECT. This project has received funding from the European Union's Horizon 2020 research and innovation ~~program~~ programme under grant agreement No ~~.~~869304~~(PROTECT).~~, PROTECT contribution number 138. JDR was supported by a UKRI Future Leaders Fellowship under grant ~~No~~ number MR/W011816/1.

References

445 Adusumilli, S., Fricker, H. A., Medley, B., Padman, L., and Siegfried, M. R.: Interannual variations in meltwater input to the Southern Ocean from Antarctic ice shelves, Nature Geoscience, 13, 616–620, https://doi.org/10.1038/s41561-020-0616-z, number: 9 Publisher: Nature Publishing Group, 2020.

Asay-Davis, X., Bull, C. Y. S., Cornford, S., Cougnon, E., De Rydt, J., Galton-Fenzi, B. K., Gladstone, R., Goldberg, D., Gwyther, D., Jordan, J., Jourdain, N., Leguy, G., Lipscomb, W., Marques, G., Martin, D. F., Nakayama, Y., Naughten, K. A., Smith, R. S.,
450 Seroussi, H., and Zhao, C.: Analysis of the Marine Ice Sheet-Ocean Model Intercomparison Project first phase (MISOMIP1), other, pico, https://doi.org/10.5194/egusphere-egu21-11918, 2021.

Asay-Davis, X. S., Cornford, S. L., Durand, G., Galton-Fenzi, B. K., Gladstone, R. M., Gudmundsson, G. H., Hattermann, T., Holland, D. M., Holland, D., Holland, P. R., Martin, D. F., Mathiot, P., Pattyn, F., and Seroussi, H.: Experimental design for three interrelated marine ice sheet and ocean model intercomparison projects: MISMIP v. 3 (MISMIP +), ISOMIP v. 2 (ISOMIP +) and MISOMIP v. 1 (MISOMIP1),
455 Geoscientific Model Development, 9, 2471–2497, https://doi.org/10.3929/ethz-b-000119139, accepted: 2019-05-29T08:09:29Z Publisher: Copernicus Publications, 2016.

Colleoni, F., Santis, L. D., Siddoway, C. S., Bergamasco, A., Golledge, N. R., Lohmann, G., Passchier, S., and Siegert, M. J.: Spatio-temporal variability of processes across Antarctic ice-bed–ocean interfaces, Nature Communications, 9, 2289, https://doi.org/10.1038/s41467-018-04583-0, 2018.

460 Cornford, S. L., Seroussi, H., Asay-Davis, X. S., Gudmundsson, G. H., Arthern, R., Borstad, C., Christmann, J., Dias dos Santos, T., Feldmann, J., Goldberg, D., Hoffman, M. J., Humbert, A., Kleiner, T., Leguy, G., Lipscomb, W. H., Merino, N., Durand, G., Morlighem, M., Pollard, D., Rückamp, M., Williams, C. R., and Yu, H.: Results of the third Marine Ice Sheet Model Intercomparison Project (MISMIP+), The Cryosphere, 14, 2283–2301, https://doi.org/10.5194/tc-14-2283-2020, publisher: Copernicus GmbH, 2020.

Danilov, S., Wang, Q., Timmermann, R., Iakovlev, N., Sidorenko, D., Kimmritz, M., Jung, T., and Schröter, J.: Finite-Element Sea Ice Model
465 (FESIM), version 2, Geoscientific Model Development, 8, 1747–1761, https://doi.org/10.5194/gmd-8-1747-2015, publisher: Copernicus GmbH, 2015.

De Rydt, J. and Gudmundsson, G. H.: Coupled ice shelf-ocean modeling and complex grounding line retreat from a seabed ridge, Journal of Geophysical Research: Earth Surface, 121, 865–880, https://doi.org/10.1002/2015JF003791, _eprint: https://onlinelibrary.wiley.com/doi/pdf/10.1002/2015JF003791, 2016.

470 De Rydt, J. and Naughten, K.: Geometric amplification and suppression of ice-shelf basal melt in West Antarctica, The Cryosphere, 18, 1863–1888, https://doi.org/10.5194/tc-18-1863-2024, 2024.

De Rydt, J., Gudmundsson, G. H., Rott, H., and Bamber, J. L.: Modeling the instantaneous response of glaciers after the collapse of the Larsen B Ice Shelf, Geophysical Research Letters, 42, 5355–5363, https://doi.org/10.1002/2015GL064355, _eprint: https://onlinelibrary.wiley.com/doi/pdf/10.1002/2015GL064355, 2015.

475 De Rydt, J., Reese, R., Paolo, F. S., and Gudmundsson, G. H.: Drivers of Pine Island Glacier speed-up between 1996 and 2016, The Cryosphere, 15, 113–132, https://doi.org/10.5194/tc-15-113-2021, publisher: Copernicus GmbH, 2021.

Dee, D. P., Uppala, S. M., Simmons, A. J., Berrisford, P., Poli, P., Kobayashi, S., Andrae, U., Balmaseda, M. A., Balsamo, G., Bauer, P., Bechtold, P., Beljaars, A. C. M., van de Berg, L., Bidlot, J., Bormann, N., Delsol, C., Dragani, R., Fuentes, M., Geer, A. J., Haimberger, L., Healy, S. B., Hersbach, H., Hólm, E. V., Isaksen, L., Kållberg, P., Köhler, M., Matricardi, M., McNally, A. P., Monge-Sanz,
480 B. M., Morcrette, J.-J., Park, B.-K., Peubey, C., de Rosnay, P., Tavolato, C., Thépaut, J.-N., and Vitart, F.: The ERA-Interim reanalysis:

configuration and performance of the data assimilation system, Quarterly Journal of the Royal Meteorological Society, 137, 553–597, https://doi.org/10.1002/qj.828, _eprint: https://onlinelibrary.wiley.com/doi/pdf/10.1002/qj.828, 2011.

Dutrieux, P., Vaughan, D. G., Corr, H. F. J., Jenkins, A., Holland, P. R., Joughin, I., and Fleming, A. H.: Pine Island glacier ice shelf melt distributed at kilometre scales, The Cryosphere, 7, 1543–1555, https://doi.org/https://doi.org/10.5194/tc-7-1543-2013, 2013.

485 Engwirda, D.: Locally optimal Delaunay-refinement and optimisation-based mesh generation, https://ses.library.usyd.edu.au/handle/2123/13148, 2014.

Engwirda, D.: JIGSAW-GEO (1.0): locally orthogonal staggered unstructured grid generation for general circulation modelling on the sphere, Geoscientific Model Development, 10, 2117–2140, https://doi.org/10.5194/gmd-10-2117-2017, publisher: Copernicus GmbH, 2017.

Favier, L., Jourdain, N. C., Jenkins, A., Merino, N., Durand, G., Gagliardini, O., Gillet-Chaulet, F., and Mathiot, P.: Assessment of sub-shelf
490 melting parameterisations using the ocean–ice-sheet coupled model NEMO(v3.6)–Elmer/Ice(v8.3), Geoscientific Model Development, 12, 2255–2283, https://doi.org/https://doi.org/10.5194/gmd-12-2255-2019, 2019.

Gladstone, R., Galton-Fenzi, B., Gwyther, D., Zhou, Q., Hattermann, T., Zhao, C., Jong, L., Xia, Y., Guo, X., Petrakopoulos, K., Zwinger, T., Shapero, D., and Moore, J.: The Framework For Ice Sheet–Ocean Coupling (FISOC) V1.1, Geoscientific Model Development, 14, 889–905, https://doi.org/10.5194/gmd-14-889-2021, publisher: Copernicus GmbH, 2021.

495 Goldberg, D., Holland, D. M., and Schoof, C.: Grounding line movement and ice shelf buttressing in marine ice sheets, Journal of Geophysical Research: Earth Surface, 114, https://doi.org/10.1029/2008JF001227, _eprint: https://onlinelibrary.wiley.com/doi/pdf/10.1029/2008JF001227, 2009.

Goldberg, D. N., Snow, K., Holland, P., Jordan, J. R., Campin, J. M., Heimbach, P., Arthern, R., and Jenkins, A.: Representing grounding line migration in synchronous coupling between a marine ice sheet model and a z-coordinate ocean model, Ocean Modelling, 125, 45–60,
500 https://doi.org/10.1016/j.ocemod.2018.03.005, 2018.

Gudmundsson, G. H.: Ice-shelf buttressing and the stability of marine ice sheets, The Cryosphere, 7, 647–655, https://doi.org/https://doi.org/10.5194/tc-7-647-2013, 2013.

Gudmundsson, G. H., Paolo, F. S., Adusumilli, S., and Fricker, H. A.: Instantaneous Antarctic ice sheet mass loss driven by thinning ice shelves, Geophysical Research Letters, 46, 13903–13909, https://doi.org/10.1029/2019GL085027, _eprint:
505 https://onlinelibrary.wiley.com/doi/pdf/10.1029/2019GL085027, 2019.

Gudmundsson, H.: Release Ua2023b · GHilmarG/UaSource, https://github.com/GHilmarG/UaSource/releases/tag/v2023b, 2024.

Gudmundsson, H., Krug, J., Durand, G., Favier, L., and Gagliardini, O.: The stability of grounding lines on retrograde slopes, The Cryosphere, 6, 1497–1505, http://dx.doi.org/10.5194/tc-6-1497-2012, number: 6 Publisher: Coperincus, 2012.

Hellmer, H. H. and Olbers, D. J.: A two-dimensional model for the thermohaline circulation under an ice shelf, Antarctic Science, 1, 325–336,
510 https://doi.org/10.1017/S0954102089000490, 1989.

Hirano, D., Tamura, T., Kusahara, K., Fujii, M., Yamazaki, K., Nakayama, Y., Ono, K., Itaki, T., Aoyama, Y., Simizu, D., Mizobata, K., Ohshima, K. I., Nogi, Y., Rintoul, S. R., van Wijk, E., Greenbaum, J. S., Blankenship, D. D., Saito, K., and Aoki, S.: On-shelf circulation of warm water toward the Totten Ice Shelf in East Antarctica, Nature Communications, 14, 4955, https://doi.org/10.1038/s41467-023-39764-z, publisher: Nature Publishing Group, 2023.

515 Hoffman, M. J., Begeman, C. B., Asay-Davis, X. S., Comeau, D., Barthel, A., Price, S. F., and Wolfe, J. D.: Ice-shelf freshwater triggers for the Filchner-Ronne Ice Shelf melt tipping point in a global ocean model, EGUsphere, pp. 1–29, https://doi.org/10.5194/egusphere-2023-2226, publisher: Copernicus GmbH, 2023.

Holland, D. M. and Jenkins, A.: Modeling Thermodynamic Ice–Ocean Interactions at the Base of an Ice Shelf, Journal of Physical Oceanography, 29, 1787–1800, https://doi.org/10.1175/1520-0485(1999)029<1787:MTIOIA>2.0.CO;2, 1999.

520 IPCC: Climate change 2013: the physical science basis: Working Group I contribution to the Fifth assessment report of the Intergovernmental Panel on Climate Change., 2013.

IPCC: IPCC, 2021: Climate Change 2021: The Physical Science Basis. Contribution of Working Group I to the Sixth Assessment Report of the Intergovernmental Panel on Climate Change, Report, Cambridge University Press, Cambridge, UK, https://www.ipcc.ch/report/ar6/wg1/, iSBN: 9781009157896 Num Pages: 2391, 2021.

525 Jordan, J. R., Holland, P. R., Goldberg, D., Snow, K., Arthern, R., Campin, J.-M., Heimbach, P., and Jenkins, A.: Ocean-Forced Ice-Shelf Thinning in a Synchronously Coupled Ice-Ocean Model, Journal of Geophysical Research: Oceans, 123, 864–882, https://doi.org/10.1002/2017JC013251, _eprint: https://onlinelibrary.wiley.com/doi/pdf/10.1002/2017JC013251, 2018.

Kreuzer, M., Reese, R., Huiskamp, W. N., Petri, S., Albrecht, T., Feulner, G., and Winkelmann, R.: Coupling framework (1.0) for the PISM (1.1.4) ice sheet model and the MOM5 (5.1.0) ocean model via the PICO ice shelf cavity model in an Antarctic domain, Geoscientific
530 Model Development, 14, 3697–3714, https://doi.org/10.5194/gmd-14-3697-2021, publisher: Copernicus GmbH, 2021.

MacAyeal, D. R.: A tutorial on the use of control methods in ice-sheet modeling, Journal of Glaciology, 39, 91–98, https://doi.org/10.3189/S0022143000015744, 1993.

Malyarenko, A., Robinson, N. J., Williams, M. J. M., and Langhorne, P. J.: A Wedge Mechanism for Summer Surface Water Inflow Into the Ross Ice Shelf Cavity, Journal of Geophysical Research: Oceans, 124, 1196–1214, https://doi.org/10.1029/2018JC014594, 2019.

535 Mitchell, W. F.: 30 years of newest vertex bisection, p. 020011, Rhodes, Greece, https://doi.org/10.1063/1.4951755, 2016.

Morlighem, M., Rignot, E., Binder, T., Blankenship, D., Drews, R., Eagles, G., Eisen, O., Ferraccioli, F., Forsberg, R., Fretwell, P., Goel, V., Greenbaum, J. S., Gudmundsson, H., Guo, J., Helm, V., Hofstede, C., Howat, I., Humbert, A., Jokat, W., Karlsson, N. B., Lee, W. S., Matsuoka, K., Millan, R., Mouginot, J., Paden, J., Pattyn, F., Roberts, J., Rosier, S., Ruppel, A., Seroussi, H., Smith, E. C., Steinhage, D., Sun, B., Broeke, M. R. v. d., Ommen, T. D. v., Wessem, M. v., and Young, D. A.: Deep glacial troughs and stabilizing ridges unveiled
540 beneath the margins of the Antarctic ice sheet, Nature Geoscience, 13, 132–137, https://doi.org/10.1038/s41561-019-0510-8, number: 2 Publisher: Nature Publishing Group, 2020.

Nakayama, Y., Timmermann, R., Schröder, M., and Hellmer, H.: On the difficulty of modeling Circumpolar Deep Water intrusions onto the Amundsen Sea continental shelf, Ocean Modelling, 84, 26–34, https://doi.org/10.1016/j.ocemod.2014.09.007, 2014.

Nakayama, Y., Menemenlis, D., Schodlok, M., and Rignot, E.: Amundsen and Bellingshausen Seas simulation with optimized
545 ocean, sea ice, and thermodynamic ice shelf model parameters, Journal of Geophysical Research: Oceans, 122, 6180–6195, https://doi.org/10.1002/2016JC012538, 2017.

Nakayama, Y., Manucharyan, G., Zhang, H., Dutrieux, P., Torres, H. S., Klein, P., Seroussi, H., Schodlok, M., Rignot, E., and Menemenlis, D.: Pathways of ocean heat towards Pine Island and Thwaites grounding lines, Scientific Reports, 9, 16 649, https://doi.org/10.1038/s41598-019-53190-6, number: 1 Publisher: Nature Publishing Group, 2019.

550 Naughten, K. A., Meissner, K. J., Galton-Fenzi, B. K., England, M. H., Timmermann, R., and Hellmer, H. H.: Future Projections of Antarctic Ice Shelf Melting Based on CMIP5 Scenarios, Journal of Climate, 31, 5243–5261, https://doi.org/10.1175/JCLI-D-17-0854.1, 2018.

Naughten, K. A., Rydt, J. D., Rosier, S. H. R., Holland, P. R., and Ridley, J. K.: Two-timescale response of a large Antarctic ice shelf to climate change., https://doi.org/in press, 2021.

Pritchard, H. D., Ligtenberg, S. R. M., Fricker, H. A., Vaughan, D. G., van den Broeke, M. R., and Padman, L.: Antarctic ice-sheet loss driven
555 by basal melting of ice shelves, Nature, 484, 502–505, https://doi.org/10.1038/nature10968, 2012.

Reese, R., Albrecht, T., Mengel, M., Asay-Davis, X., and Winkelmann, R.: Antarctic sub-shelf melt rates via PICO, The Cryosphere, 12, 1969–1985, https://doi.org/https://doi.org/10.5194/tc-12-1969-2018, 2018.

Richter, O.: UaFESOM: v1.0, https://doi.org/10.5281/zenodo.10462493, 2024.

Rignot, E., Mouginot, J., Morlighem, M., Seroussi, H., and Scheuchl, B.: Widespread, rapid grounding line retreat of Pine Island, Thwaites, Smith, and Kohler glaciers, West Antarctica, from 1992 to 2011, Geophysical Research Letters, 41, 3502–3509, https://doi.org/10.1002/2014GL060140, _eprint: https://onlinelibrary.wiley.com/doi/pdf/10.1002/2014GL060140, 2014.

Schaffer, J., Timmermann, R., Arndt, J. E., Kristensen, S. S., Mayer, C., Morlighem, M., and Steinhage, D.: A global, high-resolution data set of ice sheet topography, cavity geometry, and ocean bathymetry, Earth System Science Data, 8, 543–557, https://doi.org/https://doi.org/10.5194/essd-8-543-2016, 2016.

Schelpe, C. A. O. and Gudmundsson, G. H.: Incorporating Horizontal Density Variations Into Large-Scale Modeling of Ice Masses, Journal of Geophysical Research (Earth Surface), 128, e2022JF006 744, https://doi.org/10.1029/2022JF006744, aDS Bibcode: 2023JGRF..12806744S, 2023.

Schnaase, F. and Timmermann, R.: Representation of shallow grounding zones in an ice shelf-ocean model with terrain-following coordinates, Ocean Modelling, 144, 101 487, https://doi.org/10.1016/j.ocemod.2019.101487, 2019.

Shean, D. E., Joughin, I. R., Dutrieux, P., Smith, B. E., and Berthier, E.: Ice shelf basal melt rates from a high-resolution DEM record for Pine Island Glacier, Antarctica, The Cryosphere Discussions, pp. 1–39, https://doi.org/https://doi.org/10.5194/tc-2018-209, 2018.

Siahaan, A., Smith, R. S., Holland, P. R., Jenkins, A., Gregory, J. M., Lee, V., Mathiot, P., Payne, A. J., Ridley, J. K., and Jones, C. G.: The Antarctic contribution to 21st-century sea-level rise predicted by the UK Earth System Model with an interactive ice sheet, The Cryosphere, 16, 4053–4086, https://doi.org/10.5194/tc-16-4053-2022, publisher: Copernicus GmbH, 2022.

Smith, B., Fricker, H. A., Gardner, A. S., Medley, B., Nilsson, J., Paolo, F. S., Holschuh, N., Adusumilli, S., Brunt, K., Csatho, B., Harbeck, K., Markus, T., Neumann, T., Siegfried, M. R., and Zwally, H. J.: Pervasive ice sheet mass loss reflects competing ocean and atmosphere processes, Science, 368, 1239–1242, https://doi.org/10.1126/science.aaz5845, publisher: American Association for the Advancement of Science, 2020.

Smith, R. S., Mathiot, P., Siahaan, A., Lee, V., Cornford, S. L., Gregory, J. M., Payne, A. J., Jenkins, A., Holland, P. R., Ridley, J. K., and Jones, C. G.: Coupling the U.K. Earth System Model to Dynamic Models of the Greenland and Antarctic Ice Sheets, Journal of Advances in Modeling Earth Systems, 13, e2021MS002 520, https://doi.org/10.1029/2021MS002520, _eprint: https://onlinelibrary.wiley.com/doi/pdf/10.1029/2021MS002520, 2021.

Timmermann, R. and Goeller, S.: Response to Filchner–Ronne Ice Shelf cavity warming in a coupled ocean–ice sheet model – Part 1: The ocean perspective, Ocean Science, 13, 765–776, https://doi.org/10.5194/os-13-765-2017, 2017.

Timmermann, R., Wang, Q., and Hellmer, H.: Ice shelf basal melting in a global finite-element sea ice/ice shelf/ocean model, Annals of Glaciology, 53, https://doi.org/Timmermann, R. , Wang, Q. and Hellmer, H. (2012) Ice shelf basal melting in a global finite-element sea ice/ice shelf/ocean model , Annals of Glaciology, 53 (60) . doi:10.3189/2012AoG60A156 <http://doi.org/10.3189/2012AoG60A156> , hdl:10013/epic.40279, 2012.

Van Wessem, J. M., Berg, W. J. v. d., Noël, B. P. Y., Meijgaard, E. v., Amory, C., Birnbaum, G., Jakobs, C. L., Krüger, K., Lenaerts, J. T. M., Lhermitte, S., Ligtenberg, S. R. M., Medley, B., Reijmer, C. H., Tricht, K. v., Trusel, L. D., Ulft, L. H. v., Wouters, B., Wuite, J., and Broeke, M. R. v. d.: Modelling the climate and surface mass balance of polar ice sheets using RACMO2 – Part 2: Antarctica (1979–2016), The Cryosphere, 12, 1479–1498, https://doi.org/https://doi.org/10.5194/tc-12-1479-2018, 2018.

Wang, Q., Danilov, S., Sidorenko, D., Timmermann, R., Wekerle, C., Wang, X., Jung, T., and Schröter, J.: The Finite Element Sea Ice-Ocean Model (FESOM) v.1.4: formulation of an ocean general circulation model, Geoscientific Model Development, 7, 663–693, https://doi.org/https://doi.org/10.5194/gmd-7-663-2014, publisher: Copernicus GmbH, 2014.